Cell Systems

Supplemental Information

Integrated Transcriptome and Proteome Analyses Reveal Organ-Specific Proteome Deterioration in Old Rats

Alessandro Ori, Brandon H. Toyama, Michael S. Harris, Thomas Bock, Murat Iskar, Peer Bork, Nicholas T. Ingolia, Martin W. Hetzer, and Martin Beck

Supplemental information to:
Integrated transcriptome and proteome analyses reveal organ-specific proteome deterioration in old rats

Alessandro Ori, Brandon H. Toyama, Michael S. Harris,

Thomas Bock, Murat Iskar, Peer Bork, Nicholas T. Ingolia,

Martin W. Hetzer, and Martin Beck

Content:

Supplemental Experimental Procedures

Figure S1-S7

The following supplemental material is provided separately:

Table S1. Statistics of quantified transcripts. Related to Figure 1.

Table S2. Statistics of quantified proteins Related to Figure 1.

Table S3. Functional enrichment of affected transcripts and proteins. Related to Figure 2.

Table S4. Statistics of quantified protein complexes. Related to Figure 3.

Table S5. Integration of genomics and proteomics data. Related to Figure 4.

Table S6. Statistics of quantified phosphosites. Related to Figure 5.

Table S7. Quantification of alternative splicing events. Related to Figure 6.

Supplemental Experimental Procedures

Choice of experimental design

Tissues from the same animals (n=3 for each age group) were analyzed using multiple genomics and proteomics techniques, across three different sites that were specialized in the respective types of analysis. The experimental focus was set onto the broad application of proteomic techniques with subcellular resolution and phospho proteome analysis in two different organs with differential regenerative capacity and their integration with genomics data instead of the investigations of a large number of individuals. The data thus rather capture alterations at different regulation levels across the two age groups instead variations across individuals, such as e.g. the subtle yet intimate relationship between changes in translation and protein abundance in young vs. old animals. Those would not have been discovered using a single technique on a larger number of samples.

Explanation of figures stated in Summary

The 468 differences in protein abundance stated in the Summary indicate the cumulative number of significantly affected comparisons between young and old animals in the two organs investigated. Since a given protein group can be significant in more than one comparison, e.g. two sub-cellular fractions or both organs, the number of unique protein groups affected is slightly lower (457).

The 130 proteins not altered in their protein abundance, but affected at different levels of regulation include: 109 proteins affected at the level of phosphorylation, but not at the level of protein abundance (Figure S4D); 9 proteins undergoing changes of subcellular localization (Figure 5B); 12 proteins for which we detected an alteration of splicing and the proteomic measurement indicated no significant alteration of the overall protein abundance in the same organ. Cases that were not quantified in proteomic experiments were not considered since we cannot exclude an alteration of their protein abundance between young and old animals to occur.

Tissue fractionation

Entire organs were used for genomic and proteomic measurements. Samples of livers were homogenized as whole. Brains were cut into two hemispheres (sagittal plane) upon dissection, and an entire hemisphere was homogenized before fractionation.

Thus all regions of the brain were represented in proper proportion. Liver and brain nuclei were purified according to previously described protocols (Blobel and Potter, 1966; Lovtrup-Rein and McEwen, 1966). Further fractionation was based on previous descriptions (Toyama et al., 2013). Briefly, nuclei pellets were resuspended in corresponding nuclei purification buffers, and the supernatant was saved for further fractionation (S1). Mitochondria-enriched fractions were achieved by diluting nuclei pellet supernatants (S1) 5x in corresponding nuclei purification buffers with no sucrose and spinning at 13,000x *g* for 15 min. Supernatants (S2) were saved for future fractionation, and pellets were washed again with nuclei purification buffer and spun 13,000x *g* for 15 min. Pellets were resuspended in nuclei purification buffer and spun at 800x *g* for 5 min to pellet large insoluble materials and remaining nuclei. The supernatant was taken as the mitochondria enriched fraction (pn1). Cytosolic membrane enriched fractions were achieved by taking the initial mitochondrial supernatant (S2) and spinning again at 13,000x *g* for 15 min to remove any remaining mitochondria. The supernatant was taken and spun at 100,000x *g* for 20 min. The supernatant was taken as the cytoplasmic fraction (sol) and the pellet was resuspended in nuclei purification buffer and respun at 100,000x *g* for 20 min. The pellet was resuspended in nuclei purification buffer and taken as the ER-enriched fraction (pn2).

Determination of transcription and translation changes

Ribosome profiling libraries were prepared as described previously (Toyama et al., 2013). Total RNA libraries were prepared from homogenized tissue using TruSeq stranded kits with RiboZero gold (Illumina). Libraries for both ribosome profiling and total RNA were sequenced using the Illumina HiSeq platform. Mapping of RNA-Seq and ribosome profiling data was performed using TopHat (Trapnell et al., 2009), a splice-aware aligner. For differential expression analysis of ribosome profiling and total RNA sequencing, a generalized linear model (GLM) was constructed using DESeq (Anders and Huber, 2010). This analysis differentiates between specifically transcriptional and translational changes. Individual, highly variable outlier transcripts (colored red in Figure S2) were identified and removed from downstream analysis by testing for excess residual deviation between replicates (209 transcripts for brain and 281 transcripts for liver). Outlier samples were assessed by hierarchical clustering and

excluded from dispersion estimates. Significantly affected transcripts were defined using an adjusted p value cut-off of 0.01 (Table S1).

Mass spectrometry data acquisition and processing

Subcellular fraction samples were solubilized in 4 M urea, 0.2% (v/v) Rapigest (Waters), 100 mM ammonium bicarbonate by 1 min sonication, cysteines reduced with 10 mM DTT for 30 min at 37°C and alkylated with 15 mM iodoacetamide for 30 min in the dark. Proteins were digested for 4h at 37°C using 1:100 (w/w) LysC (Wako Chemicals GmbH) followed by overnight incubation with 1:50 (w/w) trypsin (Promega GmbH) upon dilution of urea to 1.5 M with HPLC-grade water. Digested peptides were desalted using C18 Macro-Spin columns (Harvard Apparatus) according to manufacturer instructions.

Samples were analyzed using a nanoAcquity UPLC system (Waters GmbH) connected online to a LTQ-Orbitrap Velos Pro instrument (Thermo Fisher Scientific GmbH). Peptides were separated on a BEH300 C18 (75 μm x 250 mm, 1.7 μm) nanoAcquity UPLC column (Waters GmbH) using a stepwise 145 min gradient between 3% and 85% (v/v) ACN in 0.1% (v/v) FA. The mass spectrometer was operated in data-dependent mode using a TOP-20 strategy where survey MS scans (m/z range 375-1,600) were acquired in the orbitrap (R = 30,000 FWHM) and up to 20 of the most abundant ions per full scan were fragmented by collision-induced dissociation (normalized collision energy = 35, activation Q = 0.250) and analyzed in the LTQ. Ion target values were 1,000,000 (or 500 ms maximum fill time) for full scans and 10,000 (or 50 ms maximum fill time) for MS/MS scans. Charge states 1 and unknown were rejected. Dynamic exclusion was enabled with repeat count = 1, exclusion duration = 60 s, list size = 500 and mass window ± 15 ppm. Data acquisition for phosphoproteomic analysis was performed using identical parameters with the exception of: stepwise gradient length: 115 min; TOP-15 strategy; multistage activation enabled using five phospho neutral loss masses (24.494, 32.659, 48.988, 65.318, and 97.977); ion target values MS/MS = 30,000; dynamic exclusion time = 30 s; repeat count = 2.

Raw files were processed using MaxQuant (version 1.2.2.5) (Cox and Mann, 2008). The search was performed using Andromeda search engine (Cox et al., 2011) against the Ensembl Rnor_5.0 protein database. The search criteria were set as follows: full

tryptic specificity was required (cleavage after lysine or arginine residues, unless followed by proline); 2 missed cleavages were allowed; carbamidomethylation (C) was set as fixed modification; oxidation (M) and acetylation (protein N-term) were applied as variable modifications, if applicable; for phosphoproteomic analysis, phosphorylation (STY) was applied as variable modification in addition; mass tolerance of 20 ppm (precursor ions) and 0.5 Da (fragment ions). The reversed sequences of the target database were used as decoy database. Peptide hits were filtered at a false discovery rate of 1% using a target-decoy strategy (Elias & Gygi, 2007). For the quantitative label-free analysis of protein abundance, the "peptides.txt" output file of the MaxQuant search was used to calculate protein abundance scores from the summed intensities of proteotypic peptides normalized by the protein molecular weight, as described in (Ori et al., 2013). Only proteins identified with at least 2 unique peptides were retained for quantitative analysis. For phosphoproteome analysis, search results were filtered using Andromeda score >= 60, Delta score > 5 and location probability of > 0.75. Only mono-phosphorylated peptides were retained for quantitative analysis. All comparative analyses were performed using R version 3.0.1 (R Core Team, 2012). Only proteins and phosphosites quantified in at least two replicates were used for relative quantification. To reduce technical variation, data was first $\log_2$-transformed and then quantile-normalized using the *preprocessCore* library (Gentleman et al., 2004). Differential expression was evaluated using the *limma* package (Smyth et al., 2005) and q values calculated using *fdrtool* (Strimmer, 2008). Two phosphopeptide samples (one each for nuc brain and pn2 brain) were detected as outliers by hierarchical clustering and excluded from downstream analysis. Significant affected proteins or phosphosites were defined by a q value cut-off of 0.1 (Table S2 and S6).

Quantification of histones H3.1 and H3.3 by targeted proteomics

We developed targeted proteomics assays for two proteotypic peptides for histone H3.1 (FQSSAVMALQEASEAYLVGLFEDTNLCAIHAK) and H3.3 (FQSAAIGALQEASEAYLVGLFEDTNLCAIHAK) as described in (Ori et al., 2014). The same nuclear samples used for shotgun analysis were analyzed using a TSQ Vantage triple quadrupole mass spectrometer (Thermo Fisher Scientific GmbH) connected to a nanoAcquity UPLC system (Waters GmbH). Digested peptides were

separated on a BEH300 C18 (75μm×250mm, 1,7μm) nanoAcquity UPLC column with a 75 min linear gradient between 3 and 35% (v/v) ACN 0.1% (v/v) FA at a flow rate of 300 nL/min. Data were recorded using an unscheduled acquisition with a fixed dwell time of 20 ms per transition. At least four transitions were recorded for each peptide and their co-elution was manually inspected. Peptide intensities were estimated using the summed intensity of all transitions and used to calculate the histone H3.1 to H3.3 ratio. Assays development, validation and peptide quantification was performed using SpectroDive (a kind gift of Biognosys AG).

Identification of differentially expressed protein complexes and protein complex members

Differential expression of protein complexes was assessed by a gene-set enrichment approach using the R package *gage* (Luo et al., 2009). Essentially, members of protein complexes were employed as gene set definitions and used to query the protein abundance data. *gage* was used to identify protein complexes that had members displaying consistent abundance changes (either increased or decreased abundance) during aging. The consistent expression change of the members of the same protein complex was interpreted as a change in complex abundance. A q value cut-off of 0.1 was used to determine significantly affected protein complexes.

To investigate compositional rearrangements of protein complexes rather than changes in overall complex abundance, we adapted a two-step normalization method that we described previously (Ori et al., 2013). For each sample set, we extracted protein complex members and performed a complex-wise normalization (Ori et al., 2013) by subtracting from the abundance value of each protein the trimmed-mean abundance of the rest of the complex members. In case of proteins involved in multiple complexes, the average value from all the corresponding complexes was taken into consideration. After complex-wise normalization, the relative abundance of complex members was compared in young and old animals using *limma* (Smyth, 2005) and *fdrtool* (Strimmer, 2008), as described for protein abundance (see above). A q value cut-off of 0.2 was used to determine differentially expressed complex members (Table S4).

For both approaches, we used definitions covering 270 large protein complexes curated from different resources (Ruepp et al., 2010; Vinayagam et al., 2013) and the

literature (Ori A, Iskar M, in preparation) were used. Only protein complexes that had at least 5 members quantified were considered.

Reconstruction of functional networks that are altered between young and old animals

Functional networks were reconstructed by combining alterations observed at the level of translation output, protein abundance or phosphorylation. Protein interactions were derived from STRING using a confidence score > 0.7 (Jensen et al., 2009), network modules extracted using MCODE (Bader and Hogue, 2003), and module functional enrichment assessed using ClueGO (Bindea et al., 2009).

Quantification of alternative expression of splicing isoforms

Analysis of differential splicing was performed using MISO in "isoform-centric" mode (Katz et al., 2010). Because MISO does not natively handle replicates, an analysis of merged alignments as well as each possible pairwise comparison was performed. Significantly changed transcripts were identified by Bayes factor ≥ 10, difference ≥ 0.2 in merged analysis and 5/9 pairwise comparisons and ≥ 100 counts total in merged analysis (Table S7).

Supplemental references

Anders, S., and Huber, W. (2010). Differential expression analysis for sequence count data. Genome Biol *11*, R106.

Bader, G.D., and Hogue, C.W. (2003). An automated method for finding molecular complexes in large protein interaction networks. BMC Bioinformatics *4*, 2.

Bindea, G., Mlecnik, B., Hackl, H., Charoentong, P., Tosolini, M., Kirilovsky, A., Fridman, W.H., Pages, F., Trajanoski, Z., and Galon, J. (2009). ClueGO: a Cytoscape plug-in to decipher functionally grouped gene ontology and pathway annotation networks. Bioinformatics *25*, 1091-1093.

Blobel, G., and Potter, V.R. (1966). Nuclei from rat liver: isolation method that combines purity with high yield. Science *154*, 1662-1665.

Cox, J., and Mann, M. (2008). MaxQuant enables high peptide identification rates, individualized p.p.b.-range mass accuracies and proteome-wide protein quantification. Nat Biotechnol *26*, 1367-1372.

Cox, J., Neuhauser, N., Michalski, A., Scheltema, R.A., Olsen, J.V., and Mann, M. (2011). Andromeda: a peptide search engine integrated into the MaxQuant environment. J Proteome Res *10*, 1794-1805.

Gentleman, R.C., Carey, V.J., Bates, D.M., Bolstad, B., Dettling, M., Dudoit, S., Ellis, B., Gautier, L., Ge, Y., Gentry, J., *et al*. (2004). Bioconductor: open software development for computational biology and bioinformatics. Genome Biol *5*, R80.

Jensen, L.J., Kuhn, M., Stark, M., Chaffron, S., Creevey, C., Muller, J., Doerks, T., Julien, P., Roth, A., Simonovic, M., *et al*. (2009). STRING 8--a global view on proteins and their functional interactions in 630 organisms. Nucleic Acids Res *37*, D412-416.

Katz, Y., Wang, E.T., Airoldi, E.M., and Burge, C.B. (2010). Analysis and design of RNA sequencing experiments for identifying isoform regulation. Nat Methods *7*, 1009-1015.

Lovtrup-Rein, H., and McEwen, B.S. (1966). Isolation and fractionation of rat brain nuclei. J Cell Biol *30*, 405-415.

Lu, T., Pan, Y., Kao, S.Y., Li, C., Kohane, I., Chan, J., and Yankner, B.A. (2004). Gene regulation and DNA damage in the ageing human brain. Nature *429*, 883-891.

Luo, W., Friedman, M.S., Shedden, K., Hankenson, K.D., and Woolf, P.J. (2009). GAGE: generally applicable gene set enrichment for pathway analysis. BMC Bioinformatics *10*, 161.

Ori, A., Andres-Pons, A., and Beck, M. (2014). The use of targeted proteomics to determine the stoichiometry of large macromolecular assemblies. Methods Cell Biol *122*, 117-146.

Ori, A., Banterle, N., Iskar, M., Andres-Pons, A., Escher, C., Khanh Bui, H., Sparks, L., Solis-Mezarino, V., Rinner, O., Bork, P., *et al*. (2013). Cell type-specific nuclear pores: a case in point for context-dependent stoichiometry of molecular machines. Mol Syst Biol *9*, 648.

R Core Team (2012). R: A Language and Environment for Statistical Computing (Vienna, Austria: R Foundation for Statistical Computing).

Ruepp, A., Waegele, B., Lechner, M., Brauner, B., Dunger-Kaltenbach, I., Fobo, G., Frishman, G., Montrone, C., and Mewes, H.W. (2010). CORUM: the comprehensive resource of mammalian protein complexes-2009. Nucleic Acids Res *38*, D497-D501.

Smyth, G.K. (2005). Limma: linear models for microarray data. In Bioinformatics and Computational Biology Solutions Using R and Bioconductor, C.V. Gentleman R, Dudoit S, Irizarry R and Huber W (eds.), ed. (Springer, New York), pp. 397-420.

Smyth, G.K., Gentleman, R., Carey, S., Dudoit, R., Irizarry, R., and Huber, W. (2005). Limma: linear models for microarray data (Springer).

Strimmer, K. (2008). fdrtool: a versatile R package for estimating local and tail area-based false discovery rates. Bioinformatics *24*, 1461-1462.

Toyama, B.H., Savas, J.N., Park, S.K., Harris, M.S., Ingolia, N.T., Yates, J.R., 3rd, and Hetzer, M.W. (2013). Identification of long-lived proteins reveals exceptional stability of essential cellular structures. Cell *154*, 971-982.

Trapnell, C., Pachter, L., and Salzberg, S.L. (2009). TopHat: discovering splice junctions with RNA-Seq. Bioinformatics *25*, 1105-1111.

UniProt Consortium (2009). The Universal Protein Resource (UniProt) in 2010. Nucleic Acids Res *38*, D142-148.

Vinayagam, A., Hu, Y., Kulkarni, M., Roesel, C., Sopko, R., Mohr, S.E., and Perrimon, N. (2013). Protein complex-based analysis framework for high-throughput data sets. Sci Signal *6*, rs5.

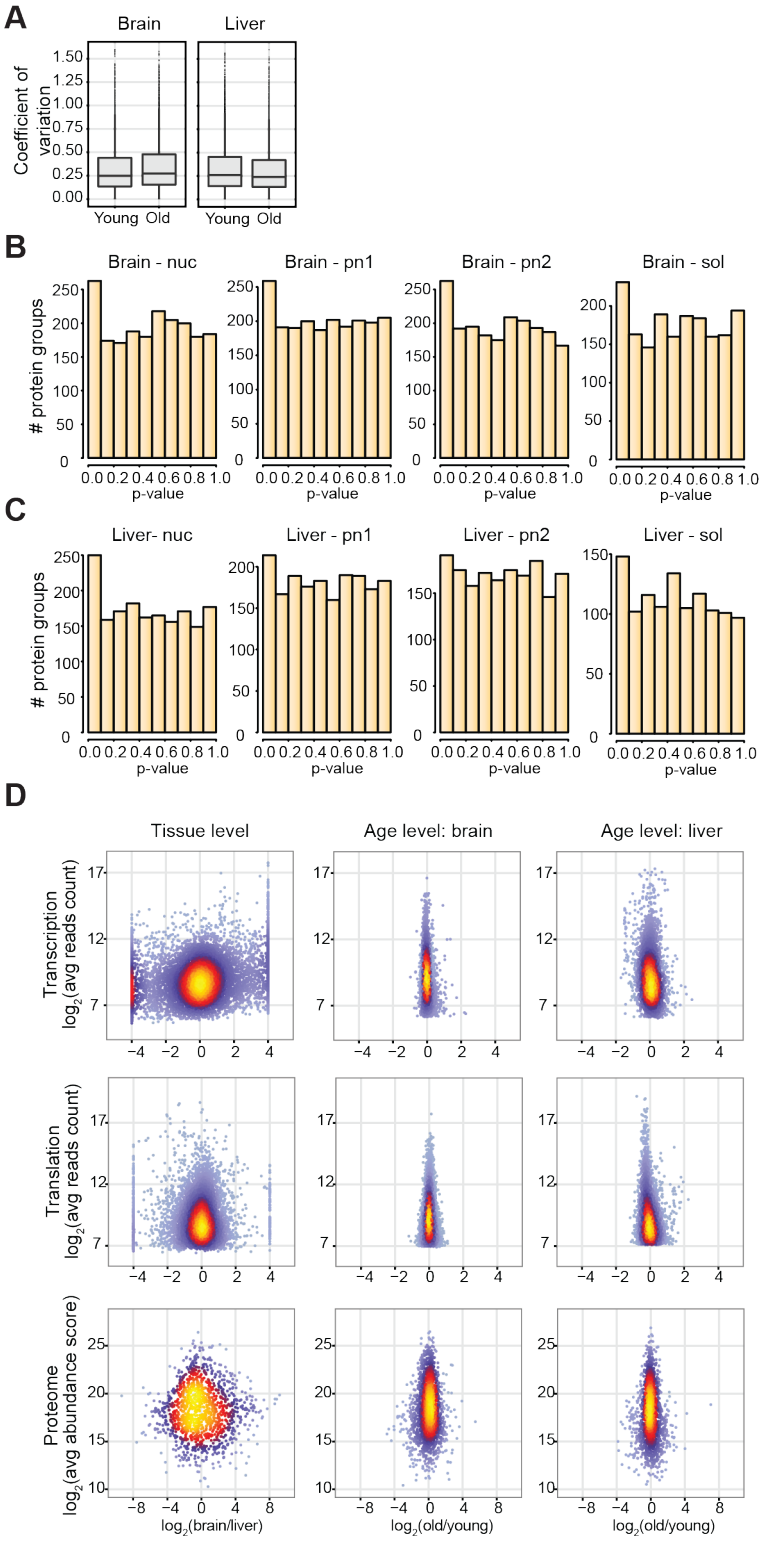

Figure S1 related to Figure 1. Reproducibility of proteomic measurements and variation of protein abundances between animals of different age. (A) Coefficients of variation (standard deviation / mean calculated on raw protein abundance scores) between animals of the same age were computed for all the protein

groups quantified across subcellular fractions. The low coefficients of variation indicate minimal within-age-group variation in protein abundance both in brain and liver. (B and C) Distribution of p values for all the subcellular fractions analyzed. The enrichment of protein groups having low p values (< 0.1) indicates deviation from the null-hypothesis (i.e. presence of proteins that vary in abundance between young and old animals). As discussed in the manuscript, brain samples are generally more affected than liver one. P values were calculated using *fdrtool* (Strimmer, 2008) from the t-statistics computed by *limma* (Smyth *et al* 2005). (D) Molecular alterations during physiological aging are mild. The effect of aging at the level of transcription, translation output and protein abundance is compared to differences between the two organs. Age-related changes are characterized by small effect sizes and they affect a limited number of transcripts and proteins. For proteomic data, the comparison of the nuclear fractions is shown as a representative example.

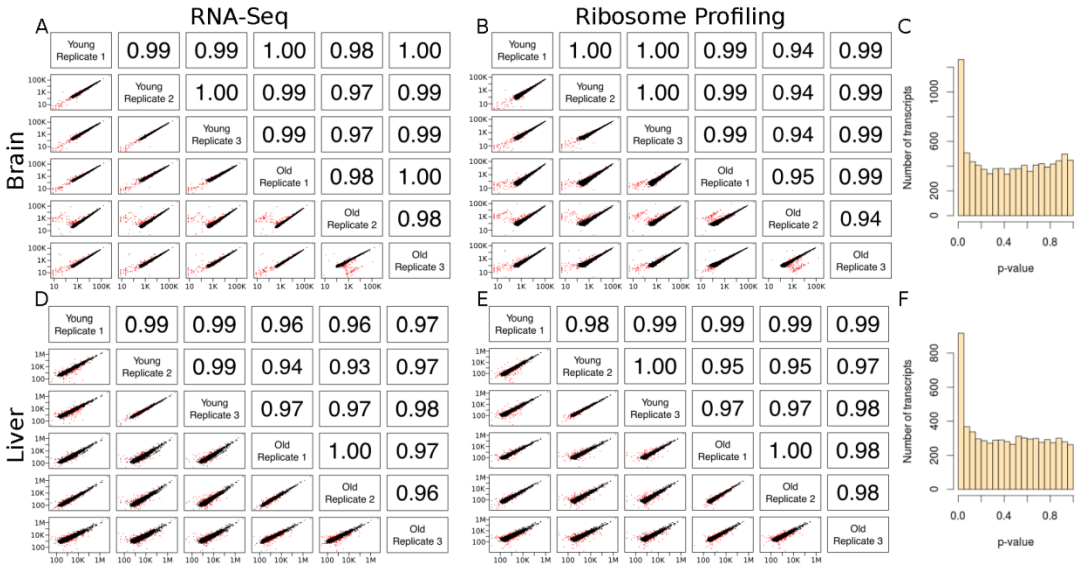

Figure S2 related to Figure 1. Replicate samples of RNA-Seq and Ribosome Profiling are consistent. (A-B, D-E) Pairwise scatterplots and Pearson correlations are given for RNA-Seq (A, D) and Ribosome Profiling (B, E) counts. Samples from different animals show high correlation in both measurements for both tissues. Points in red were filtered from final analysis due to high dispersion (see Supplemental Experimental Procedures for details). (C, F) Distribution of p values for translation output in brain (C) and liver (F). Enrichment of low p values indicates statistically significant changes.

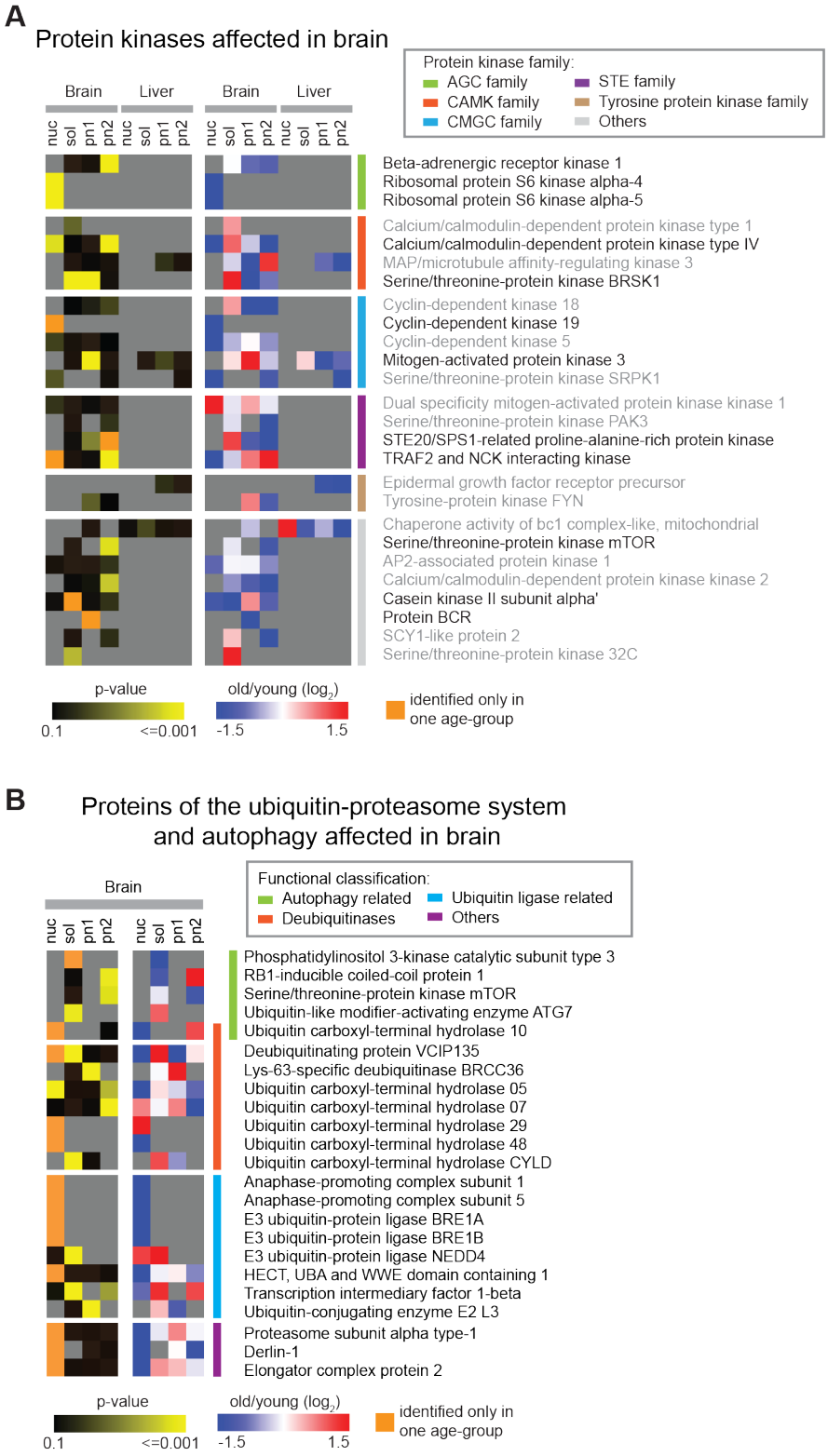

Figure S3 related to Figure 2. Protein kinases and members of the ubiquitin-proteasome system and autophagy are affected between young and old animals. (A) Kinases are grouped in families as classified in UniProt (UniProt Consortium, 2009). The names of twelve significantly affected cases (q value < 0.1) are indicated

in black font, while the names of additional 14 kinases that showed a strong trend (p value < 0.05) but did not raise to significant level (q value > 0.1) are indicated in gray font. (B) Several proteins functionally related to the ubiquitin proteasome system and autophagy change abundance in brain from old animals. Proteins are grouped according to their functional classification. See also Table S2.

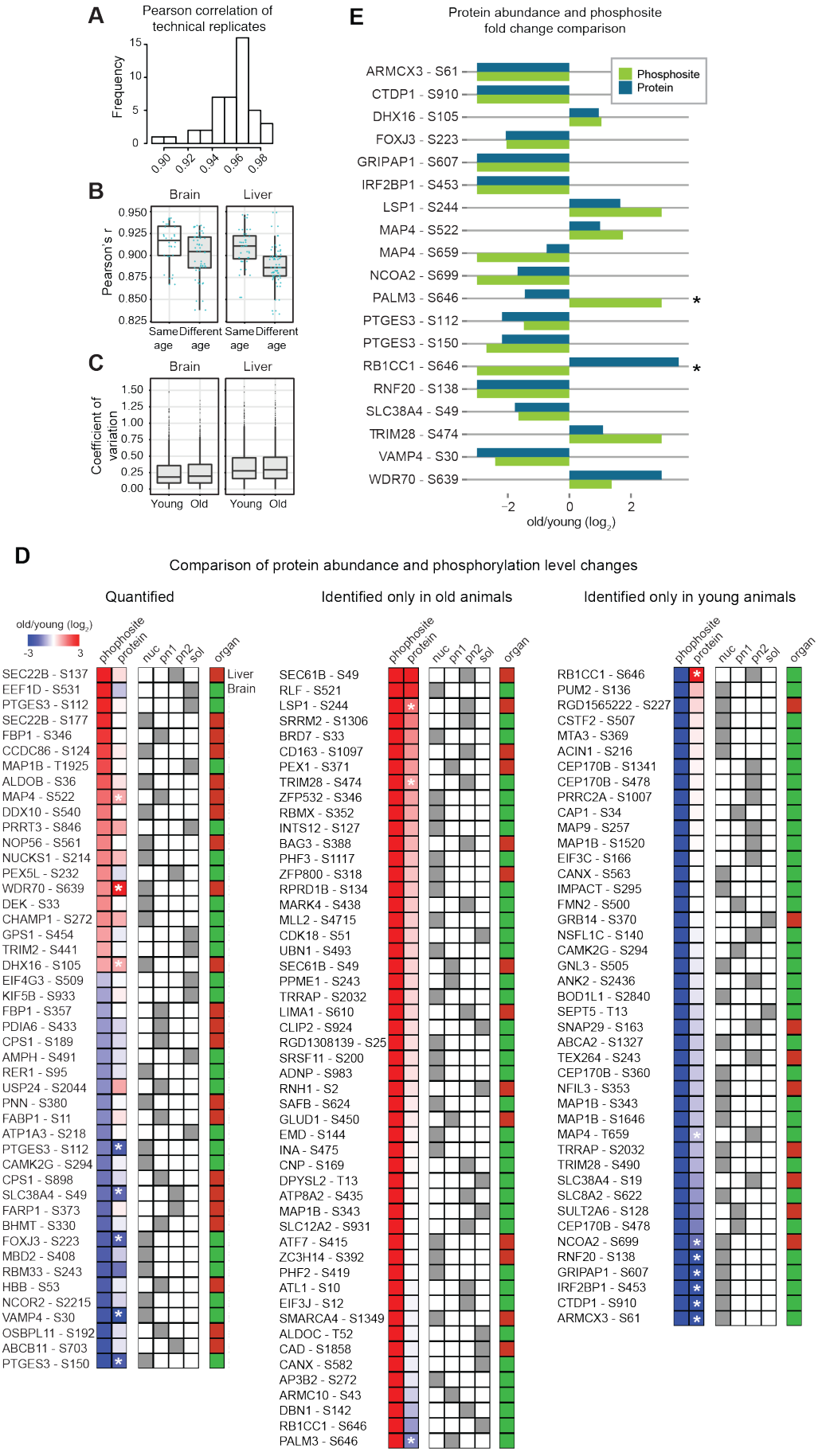
A
Pearson correlation of technical replicates
Frequency
B
Brain
Liver
Pearson's r
Same age
Different age
C
Coefficient of variation
Young
Old
E
Protein abundance and phosphosite fold change comparison
Phosphosite
Protein
ARMCX3 - S61
CTDP1 - S910
DHX16 - S105
FOXJ3 - S223
GRIPAP1 - S607
IRF2BP1 - S453
LSP1 - S244
MAP4 - S522
MAP4 - S659
NCOA2 - S699
PALM3 - S646
PTGES3 - S112
PTGES3 - S150
RB1CC1 - S646
RNF20 - S138
SLC38A4 - S49
TRIM28 - S474
VAMP4 - S30
WDR70 - S639
old/young (log2)
D
Comparison of protein abundance and phosphorylation level changes
Quantified
Identified only in old animals
Identified only in young animals
old/young (log2)
phosphosite
protein
nuc
pn1
pn2
sol
organ
Liver
Brain
SEC22B - S137
EEF1D - S531
PTGES3 - S112
SEC22B - S177
FBP1 - S346
CCDC86 - S124
MAP1B - T1925
ALDOB - S36
MAP4 - S522
DDX10 - S540
PRRT3 - S846
NOP56 - S561
NUCKS1 - S214
PEX5L - S232
WDR70 - S639
DEK - S33
CHAMP1 - S272
GPS1 - S454
TRIM2 - S441
DHX16 - S105
EIF4G3 - S509
KIF5B - S933
FBP1 - S357
PDIA6 - S433
CPS1 - S189
AMPH - S491
RER1 - S95
USP24 - S2044
PNN - S380
FABP1 - S11
ATP1A3 - S218
PTGES3 - S112
CAMK2G - S294
CPS1 - S898
SLC38A4 - S49
FARP1 - S373
BHMT - S330
FOXJ3 - S223
MBD2 - S408
RBM33 - S243
HBB - S53
NCOR2 - S2215
VAMP4 - S30
OSBPL11 - S192
ABCB11 - S703
PTGES3 - S150
SEC61B - S49
RLF - S521
LSP1 - S244
SRRM2 - S1306
BRD7 - S33
CD163 - S1097
PEX1 - S371
TRIM28 - S474
ZFP532 - S346
RBMX - S352
INTS12 - S127
BAG3 - S388
PHF3 - S1117
ZFP800 - S318
RPRD1B - S134
MARK4 - S438
MLL2 - S4715
CDK18 - S51
UBN1 - S493
SEC61B - S49
PPME1 - S243
TRRAP - S2032
LIMA1 - S610
CLIP2 - S924
RGD1308139 - S25
SRSF11 - S200
ADNP - S983
RNH1 - S2
SAFB - S624
GLUD1 - S450
EMD - S144
INA - S475
CNP - S169
DPYSL2 - T13
ATP8A2 - S435
MAP1B - S343
SLC12A2 - S931
ATF7 - S415
ZC3H14 - S392
PHF2 - S419
ATL1 - S10
EIF3J - S12
SMARCA4 - S1349
ALDOC - T52
CAD - S1858
CANX - S582
AP3B2 - S272
ARMC10 - S43
DBN1 - S142
RB1CC1 - S646
PALM3 - S646
RB1CC1 - S646
PUM2 - S136
RGD1565222 - S227
CSTF2 - S507
MTA3 - S369
ACIN1 - S216
CEP170B - S1341
CEP170B - S478
PRRC2A - S1007
CAP1 - S34
MAP9 - S257
MAP1B - S1520
EIF3C - S166
CANX - S563
IMPACT - S295
FMN2 - S500
GRB14 - S370
NSFL1C - S140
CAMK2G - S294
GNL3 - S505
ANK2 - S2436
BOD1L1 - S2840
SEPT5 - T13
SNAP29 - S163
ABCA2 - S1327
TEX264 - S243
CEP170B - S360
NFIL3 - S353
MAP1B - S343
MAP1B - S1646
MAP4 - T659
TRRAP - S2032
TRIM28 - S490
SLC38A4 - S19
SLC8A2 - S622
SULT2A6 - S128
CEP170B - S478
NCOA2 - S699
RNF20 - S138
GRIPAP1 - S607
IRF2BP1 - S453
CTDP1 - S910
ARMCX3 - S61

Figure S4 related to Figure 5. Reproducibility of phosphoproteomic measurements and comparison of protein abundance and phosphorylation level changes. (A) Reproducibility of phosphopeptide abundance measurements. The reproducibility of phosphopeptide abundance measurements was assessed by correlating protein abundance scores between technical replicates. The histogram shows the distribution of pairwise correlations between all technical replicates for brain and liver. The average pairwise correlation was Pearson's r = 0.957, indicating high reproducibility. (B) As for protein abundance measurements (Figure 1C), samples from the same age group displayed consistently higher correlation than samples from different age groups. The boxplots depict all the pairwise correlations between samples from all the subcellular fractions. For both brain and liver, the correlation coefficients of samples from the same age group are significantly higher than samples from different age groups (Wilcoxon rank sum test p value 2.0e-2 and 3.2e-4, respectively). (C) Coefficients of variation (standard deviation / mean calculated on raw phosphopeptide intensities) between animals of the same age were computed for all the phosphopeptides quantified across subcellular fractions. The low coefficients of variation indicate minimal within-age-group variation in phosphopeptide levels both in brain and liver. (D) Comparison of protein abundance and phosphorylation level changes. For 136 affected phosphosites, we had measurements of both protein abundance and phosphorylation level in the same subcellular fraction. The heatmap show side–by–side comparison of protein abundance and phoshorylation level fold changes. For 19 of these phosphosites (indicated by a white star), we detected changes at both protein (p value < 0.05) and phosphopetide level. These cases are highlighted in (E): the barplot compares fold changes measured at the protein (dark blue) and phosphopeptide level (green) in the two independent experiments. In 17 out of 19 cases (90%) the fold changes measured at the protein and phosphopeptide level are in agreement (fold change with same sign). A star indicates not consistent cases that are suggestive of an alteration of the fraction of protein molecules phosphorylated. Proteins and phosphosites identified only in one age group were assigned an arbitrary $\log_2$ fold change of +3 (identified only in old animals) or -3 (identified only in young animals). See also Table S6.

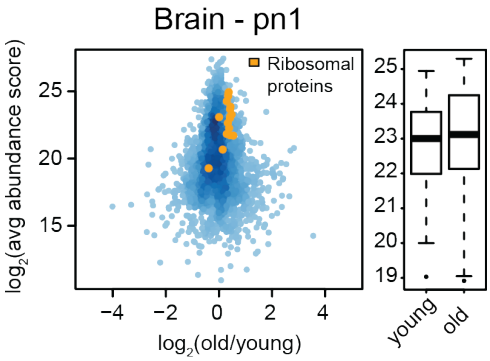

Figure S5 related to Figure 6. Increased abundance of ribosomal proteins in old brain. All proteins identified in the pn2 fraction of brain are plotted according to their average abundance score and average fold change between young and old animals (both $\log_2$-transformed). Positive values indicate higher expression in old animals and negative values indicate higher expression in young animals. Orange dots indicate the identified members of the cytosolic ribosome. Boxplots show the distribution of abundances of ribosomal proteins in young and old animals.

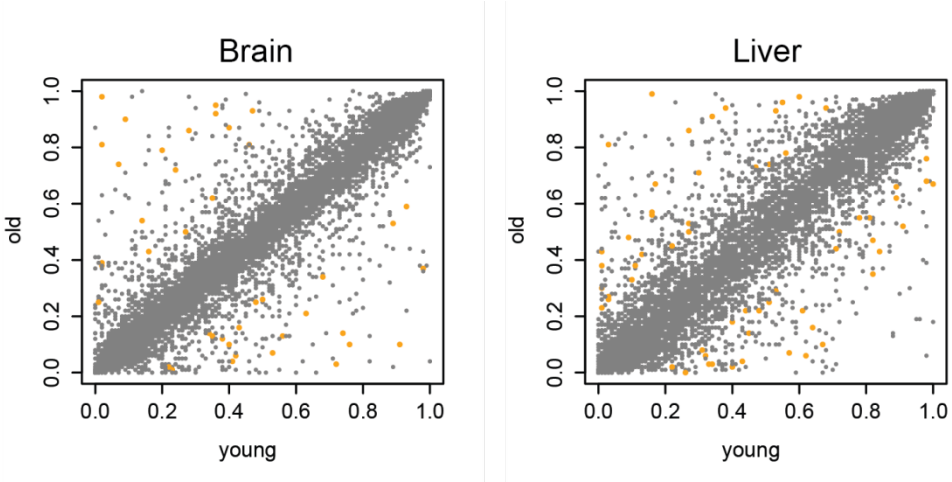

Figure S6 related to Figure 7. Changes in PSI value for all transcripts. Percent Spliced In (PSI) values are mostly consistent across age, but with a moderate number of differentially expressed transcripts. Significantly changed transcripts, marked in orange, had bayes factor ≥ 10 and difference ≥ 0.2 in merged and at least 5/9 individual analyses. See also Table S7.

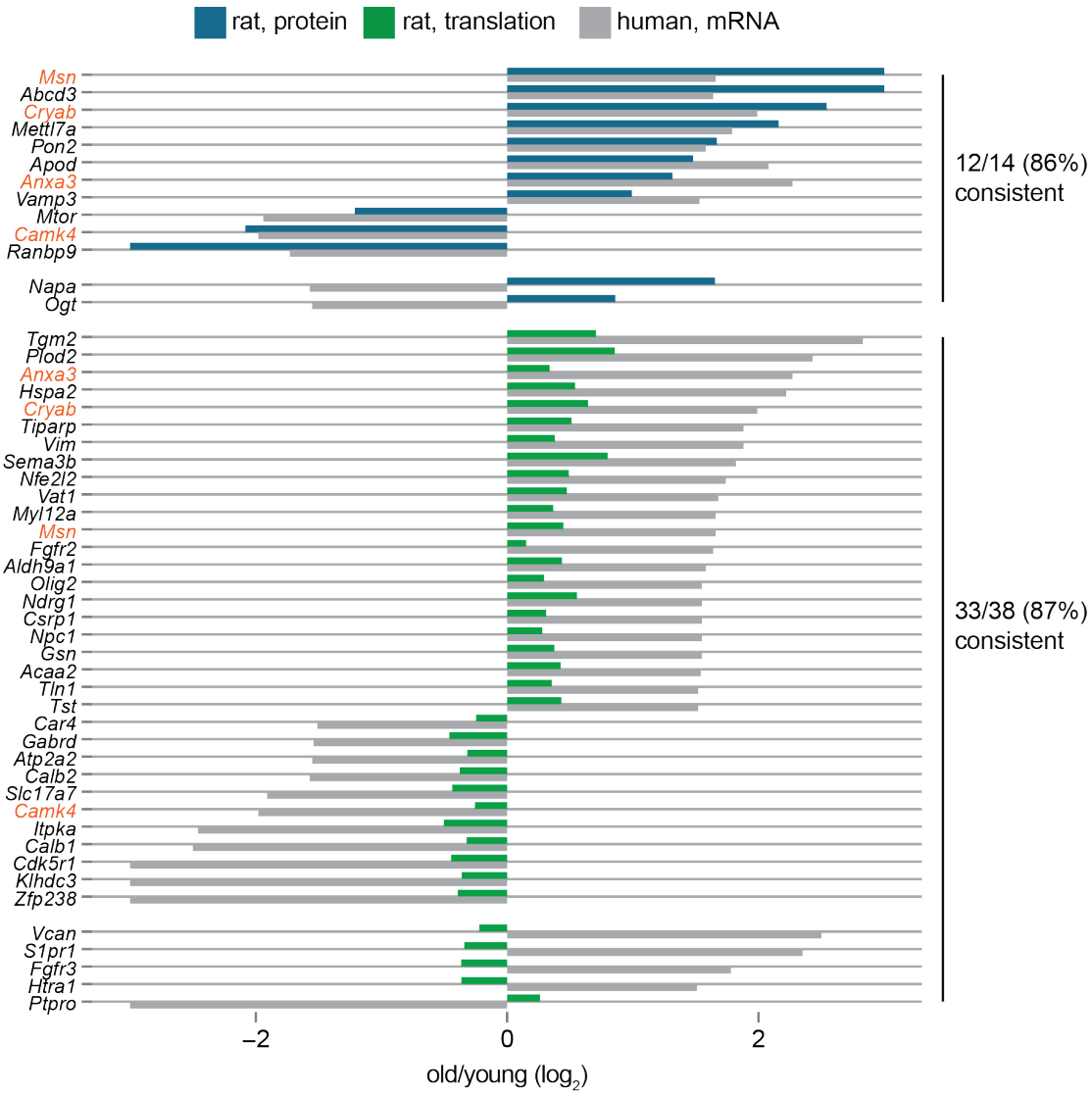

Figure S7 related to Figure 6. Conserved molecular alterations in aging brain between rat and human. We compared significant changes in protein abundance or translation output that we identified in aging rat brain to changes in transcript level associated to age in human brain (Lu et al., 2004). 12 out of 14 (86%) changes in the protein abundance level and 33 out of 38 (87%) alterations in translation output that were identified as significant in both our and the human dataset are consistent having fold changes with the same sign. This suggests that conservation of age-associated molecular events between rodents and humans. Cases that were identified as significantly affected both at the level of translation output and protein abundance are highlighted in orange.